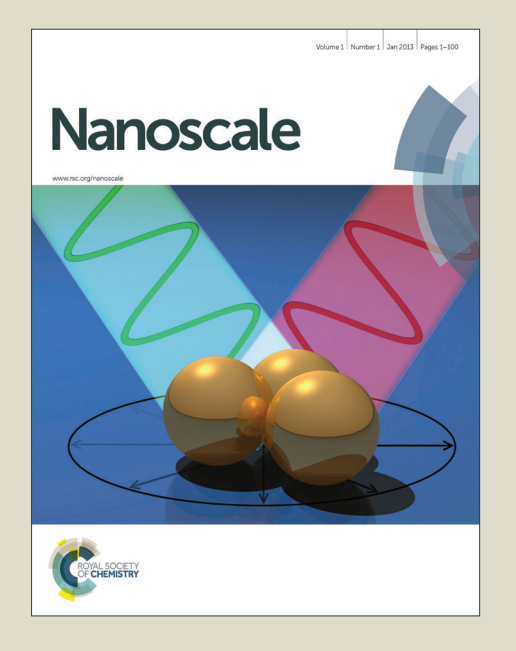
Nanoscale

Accepted Manuscript



This is an *Accepted Manuscript*, which has been through the Royal Society of Chemistry peer review process and has been accepted for publication.

Accepted Manuscripts are published online shortly after acceptance, before technical editing, formatting and proof reading. Using this free service, authors can make their results available to the community, in citable form, before we publish the edited article. We will replace this Accepted Manuscript with the edited and formatted Advance Article as soon as it is available.

You can find more information about *Accepted Manuscripts* in the **Information for Authors**.

Please note that technical editing may introduce minor changes to the text and/or graphics, which may alter content. The journal's standard <u>Terms & Conditions</u> and the <u>Ethical guidelines</u> still apply. In no event shall the Royal Society of Chemistry be held responsible for any errors or omissions in this *Accepted Manuscript* or any consequences arising from the use of any information it contains.



Cite this: DOI: 10.1039/c0xx00000x

www.rsc.org/xxxxxx

ARTICLE TYPE

Cite this: DOI: 10.1039/x0xx00000x

Received xxth xxx 2014, Accepted xxth, xxx 2014

DOI: 10.1039/x0xx00000x

www.rsc.org/

Hierarchical Porous Carbon Aerogel Derived from Bagasse for High Performance Supercapacitor Electrode

Pin Hao; A, Zhenhuan Zhao; Jian Tian, Haidong Li, Yuanhua Sang, Guangwei Yu^a, Huaqiang Cai^b, Hong Liu^a*, C. P. Wong^c*, Ahmad Umar^{d,e}*

Renewable, cost-effective and eco-friendly electrode materials have drawn much attention in energy conversion and storage fields. Bagasse, the waste product from sugarcane, mainly contains cellulose derivatives, can be a promising candidate to manufacture supercapacitor electrode materials. This study demonstrates the fabrication and characterizations of highly porous carbon aerogels by using bagasse as raw material. Macro and mesoporous carbon was firstly prepared by carbonizing the freeze drying bagasse aerogel and consequently microporous structure was created on the walls of mesoporous carbon by chemical activation. Interestingly, it was observed that the specific surface area, the pore size and distribution of the hierarchical porous carbon were affected by the activation temperature. In order to evaluate the ability of the hierarchical porous carbon towards supercapacitor electrode performance, solid state symmetric supercapacitors were assembled which demonstrated a comparable high specific capacitance of 142.1 F g⁻¹ at discharge current of 0.5 A g⁻¹. The fabricated solid state supercapacitor displayed excellent capacitance retention of 93.86% over 5000 cycles. The high energy storage ability of the hierarchical porous carbon was attributed to the specially designed pore structures, i.e., co-existence of the micropores and mesopores. This research has demonstrated that utilization of sustainable biopolymers as the raw materials for high performance supercapacitor electrode materials are the effective way to fabricate low-cost energy storage devices.

1. Introduction

Recentlty, supercapacitors, known as electrochemical capacitors (ECs), with high power density, high specific capacitance and excellent cycling stability characteristics have received considerable attention due to increased demand of energy storage devices. Typically, supercapacitors deliver a power density that is an order of magnitude larger (10000 W kg⁻¹) than that of lithium ion batteries, and an energy density that is two orders of magnitude higher (10 Wh kg⁻¹) than that of electrolytic capacitors. 1,2 Supercapacitors can be quickly charged and have ultralong lifetime even discharged at high current density. Thus, the supercapacitors have specific applications such as backup energy, electric vehicles, wind power and even replace batteries.³ The commercial supercapacitors are mainly using porous carbon as the active electrode materials but exhibit relatively low energy density.^{4,5} This is the reason why much research efforts are mainly focused on the enhancement of energy storage abilities of supercapacitors. For this, transition metal oxides and conducting polymers are widely used as active electrode materials which store electrical energy based on the redox reactions.⁶⁻⁹ However, supercapacitors using transition metal oxides and conducting polymers possess poor cyclability and rate capability, despite of high energy density and specific capacitance. Research has thus been focused on increasing energy density without sacrificing cycle life or high power density.

The energy storage ability of a supercapacitor is determined by the choice and structure of active electrode materials. 10 Mostly, carbon materials including activated carbon, carbon fibers, carbon nanotubes, carbon aerogels, graphene and carbide-derived carbons are widely used as active electrode materials. 11-19 These carbon materials have very good supercapacitor behavior. However, most of them are prepared from mineral materials and petroleum, which are thought to be used up in the very near future. The expensive costs of raw materials, environmental destructiveness of preparation and complicated manufacturing largely limit the further applications of most supercapacitors. Thus, researches were focused on the utilization of green reproducible biomass or their derivatives to produce porous carbon materials which are critical to the sustainable development and environmental protection.^{20,21} Accordingly, much efforts have been done to prepare carbon based on natural sources such as carbonization of chicken feather and banana peel for energy storage devices.²²⁻²⁹ Eventhough various carbon based materials were prepared by a variety of natural ways and used for energy

storage devices but unlikely, the electrochemical performances of the fabricated devices were not satisfactory.

Different from other reported literature, the present research demonstrates the fabrication of hierarchical porous carbon materials using bagasse as raw material. Bagasse is the industrial waste of sugar refining industries which is produced after sucrose extraction from the sugarcane plant. Bagasse has high proportion of cellulose and hence presents itself as potential and interesting candidate for the production of porous carbon electrode materials. 30 Bagasse originates from abundant and essentially free renewable biomasses, and with the growing demand of sugar, much more bagasse will be produced as the industrial waste.

Unlike to the proposed idea presented in this paper, in the previous literatures, cellulose was utilizated as the supporting materials and substrates which mainly took the advantages of mechanical properties and flexibility of cellulose. 31-33 However. these ideas still could not make full use of cellulose to prepare the all-carbon materials, such as carbon nanotube, graphene, etc, which are expensive. Therefore, converting bagasse into electrode material is supposed to be an economical and environmentally friendly route.

For the structure of carbon materials, the electrochemical performance of ECs is dependent upon several parameters, such as the electric conductivity of the electrode materials, pore size and distribution, specific surface area and so on. The electric conductivity affects the power density that ECs can deliever. The specific surface area and pore size affects the specific capacitance and energy density. For example, the KOH activated porous graphene exhibited very high specific surface area (3100 m² g⁻ 1).³⁴ However, the increase of the specific surface area can not always positively enhance the specific capacitance. Because with increasing the specific surface area, the pore volume of micropores increases and the size of the micropores decreases to below the size of hydrated electrolyte ions, which decreases the accessibility of pores.3 The ideal ECs electrode materials should have a hierarchical porous structure containing macropores (larger than 50 nm) for the ion-buffering reservoir, mesopores (2-50 nm) for ion transportation and micropores (less than 2 nm) for the enhancement of the charge storage. Moreover, it is also desirable that the porous carbon structures should have multiscale pores.³⁵

In this study, hierarchical porous carbon aerogels were prepared from freeze drying cellulose aerogels using bagasse as the raw material. The direct carbonization of cellulose aerogel created numerous macro and mesopores. A post KOH activation process which is widely used for manufacturing porous carbon was employed to produce micropores on the walls of the mesoporous carbon aerogels. Therefore, the present work provides a general hit for the utilization of sustainable materials for hierarchical porous carbon used for supercapacitors, which is effective, easily to be operated, low cost, and environmental friendly. The special hierarchical porous structures demonstrate high electrochemical performances and various fascinating advanatages such as bagasse, the raw material is the industrial waste which can be efficiently utilized for large-scale production of hierarchical porous carbon materials.

Furthermore, the prepared hierarchical carbon aerogels possess high specific surface area with reasonable pore size distributions and hence exhibited good energy storage performances and high cycling stabilities. Moreover, the effects of the activation temperatures on the pore size distribution were also investigated and their corresponding electrochemical performances were compared. Finally, the real supercapacitive performances of hierarchical carbon aerogel with opitimized condictions were studied using an all-solid-state supercapacitor.

2. Experimental

2.1 Materials

The bagasse was obtained from the sugarcanes (purchased from the supermarket) which were dried under laboratory conditions and then dried again at 100 °C. The cellulose used in this study was extracted from the above bagasse. All other chemicals were of reagent grade and used without further purification. Deionized water was used throughout the experiments.

2.2 Preparation of cellulose aerogel

The cellulose was purified from the bagasse by an alkaline hydrolysis, according to the reported method.³⁶ Initially, in order to remove the lignin and hemi cellulose, the dried bagasse was kept at 80 °C in 4 % sodium hydroxide solution for 4 h. Following the persistent discoloration of the product bleached with a sodium chlorite/glacial acetic acid mixture, the residual lignin and hemi cellulose were removed. The bleached cellulose fibers were washed repeatedly to attain a neutral pH. Then cellulose aerogel was prepared as follows. The first step was the dissolution of cellulose in which the solvent mixture of NaOH/urea/H₂O (7.5:11.5:81w/w) was precooled to -12 °C and the desired amount (7 wt%) of the cellulose was dispersed into the solvent system under vigorous stirring for 4 h at -6 °C to obtain a transparent cellulose sol. Then the mixture was kept for 12 hours at 50 °C to ensure complete gelation. Secondly, the gels were regenerated in water at room temperature which were then frozen to -80 °C for 12 h and dried using freeze-dryer.

2.3 Preparation and activation of carbon aerogel

The resultant cellulose aerogels were pyrolyzed at 800 °C for 3 h under flowing N₂. The obtained carbon aerogels were then mixed with KOH solution at KOH/carbon aerogel weight ratio of 3:1 under vigerous stirring. After stirring for 2 h, the mixture was then dried at 110 °C to prepare the impregnated sample which was then heated up to various temperatures under N₂ flow for 2 h. The activation temperatures were varied from 700 °C to 900 °C (samples are denoted as K700, K800, K900). After heating at particular temperatures, the samples were cooled to roomtemperature under contineous N2 flow. The obtained samples were washed thoroughly with deionized water in order to remove the residual chemicals. Finally, the activated carbon aerogels were obtained after drying the prepared samples at 50 °C for 12 h.

2.4 Characterizations of hierarchical porous carbon aerogels

The morphologies and structural properties of the prepared materials were characterized by field emission scanning electron microscopy (FESEM; HITACHI S-4800) and transmission electron microscopy (TEM; JEOL JEM2100F) equipped with high-resolution imaging features. The scattering and further

Page 3 of 10 Nanoscale

structural properties were investigated by Raman-scattering (Jobin-Yvon HR 800) spectrometer.

The porous characteristics of the prepared materials were examined by N_2 adsorption/desorption experiments at 77 K using ASAP 2020 V3.02 H. The specific surface area was measured according to the Brunauer-Emmett-Teller (BET) method, and the BJH model was used to calculate the pore size distribution and pore volumes.

2.5 Electrochemical measurements

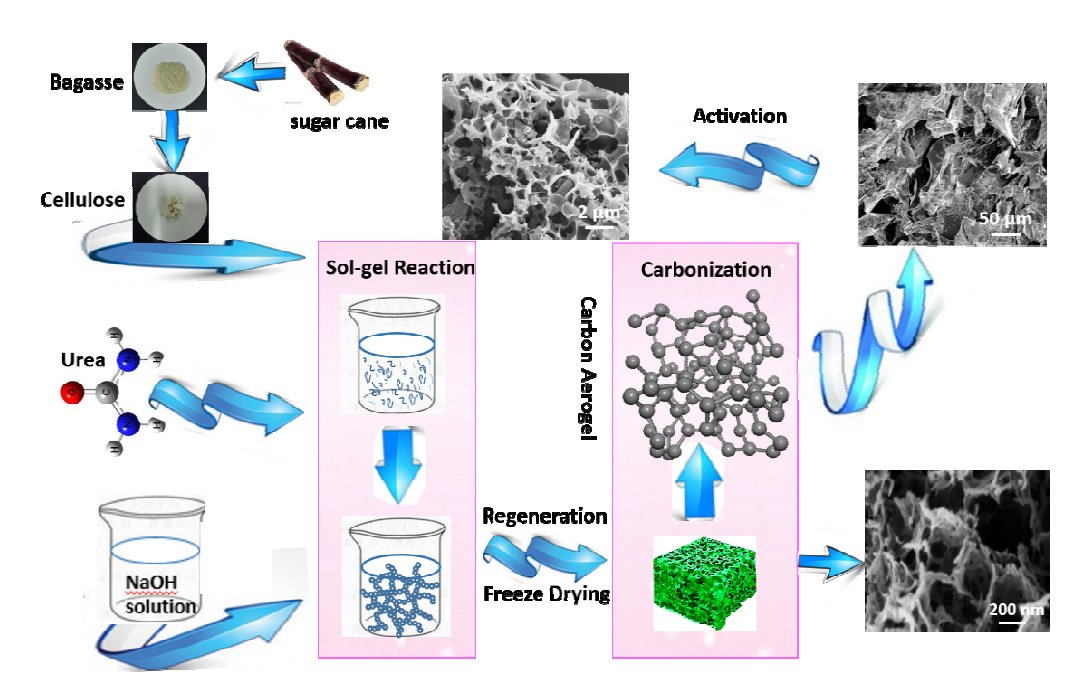
To obtain the electrochemical properties of the prepared samples, three-electrode configurations and two-electrode configurations were used. To prepare the electrode used in the three electrode set-up, according to the conventional optimization methods, the supercapacitor electrodes were made of different activated carbon aerogels, acetylene black and polyvinylidenefluoride (PVDF).³⁷ Prior to prepare the electrode, PVDF were added into N-methyl pyrrolidinone (NMP) solution(0.01 g ml⁻¹), and then the carbon aerogel and acetylene black were added to the above solution with the carbon aerogel/acetylene black/PVDF weight ratio of 8:1:1. After stirring for 12 h, the mixture was pressed onto a nickel foil with a size of 1 cm x 1 cm. And then, the prepared electrodes were dried at 60 °C in air for 12 h to remove NMP solution. In a conventional three-electrode cell, a Pt wire and a planar Ag/AgCl (saturated with KCl (aq)) were used as the counter and reference electrodes, respectively. Aqueous solution of 6 M KOH was used as the electrolyte. To evaluate the performance of the activated carbon aerogel as two symmetrical electrodes, two-electrode configuration was used.

To prepare the KOH/PVA gel electrolyte, 4.5 g of KOH was added into 60 mL of deionized water and then 6 g of PVA was also added in it. The mixture was then heated to 85 °C under continueous stirring until the solution became clear. Two electrodes, made by the above mentioned method were immersed into the KOH/PVA solution for 5 min, keeping the foil without carbon materials above the solution, and then overlaid the two electrodes head to head until solidified the gel at room temperature.

Cyclic voltammetric (CV), galvanostatic charging/discharging measurements (GCD) and electrochemical impedance spectroscopy (EIS) were performed by using a CHI 660C Electrochemical Workstation (CH Instruments, China).

3. Results and Discussion

The main process of preparing hierarchical porous carbon aerogels derived from bagasse is schematically illustrated in Scheme 1. The first step is the dissolution of cellulose fibers, which involved the purification of cellulose from bagasse. This solution was then placed for a few hours to form the gel, and kept in water for regeneration. Following the freeze drying and carbonization process, carbon aerogels can be obtained. To further optimize the pore size distribution and prepare hierarchical porous structures, the obtained carbon aerogels were then mixed with KOH solution, after dried at 110 °C, the mixture was activated at different temperatures under N₂ flow for 2 h. The resulting mixture was then washed and dried, yielding hierarchical nanoporous structures. Figure S1 demonstrate the systematic and detailed processess for the fabrication of bagasse-derived carbon aerogels.



Scheme 1. Schematic of the fabrication of highly porous bagasse-derived carbon aerogels with hierarchical pore structure.

To examine the general morphologies, all the prepared carbon aerogel samples were examined by FESEM and results are

demonstrated in Figure 1. Figure 1 depicts the general morphologies of the as-synthesized carbon aerogels with and

without post activation treatments. The observed FESEM images shown in figure 1 (a) and (b) clearly reveal that the carbon aerogels possess porous structures which exhibit large channels with the avearage diameters in the range of 50-100 µm. It is also clear from the observed FESEM images that the channels are well connected with each other which is promising for the electrolyte ions diffusion. The morphology of as-obtained cellulose aerogels (Figure S2) is different with that after carbonization. Before carbonization, cellulose aerogels possess well-shaped mecroporous structures, with channel diameters are in the range of 450 ± 50 nm. Interestigly, the channels exhibit uniform diameter distribution which is the typical characteristic of aerogels. After carbonization, the uniform porous structures of cellulose aerogels were broken and the macropores reassemble together to form large particles and left with very large crackes, and transferred to porous structure with pore sizes in the range of $80 \pm 20 \mu m$. The high resolution SEM image of carbonized aerogel confirmed that there was no secondary pores in the aerogels (Figure 1 (b)). The transformation to such a porous structure with $80 \pm 20 \mu m$ diameters of pores was caused by the local melting of cellulose and then carbonization of the cellulose aerogel during the heating and carbonization process. It is well known that the glass transition temperature of dried cellulose is ~200 °C, 38 and when the sample was heated to ~200 °C, the melting process of the cellulose causes the connection of the cellulose molecules, and form complete surface in some part of the aerogels due to the high surface tension. Because of the lack of enough mass of cellulose of the porous aerogels, the aerogels cannot connect to be an entire bulk structures, and the network is broken and forms porous structure with very large pores. Figure 1 (c)-(f) demonstrate the typical FESEM images of the carbon aerogels after activation. As shown in the images, all three samples show the presence of open and interconnected pores, forming a three-dimensional macroporous framework. When the sample was activated at 700°C, the carbon aerogels display an uninterrupted 3D networks constructed with carbon walls from the carbonization of biopolymers of cellulose, and the pore sizes were less than 2 µm, much smaller than those in the ascarbonized sample (Figure 1 (c) and (d)). However, when the activation temperatures increase to 800 °C (Figure 1(e)) and 900 °C (Figure 1(f)), three-dimensional macroporous frameworks were unchanged.

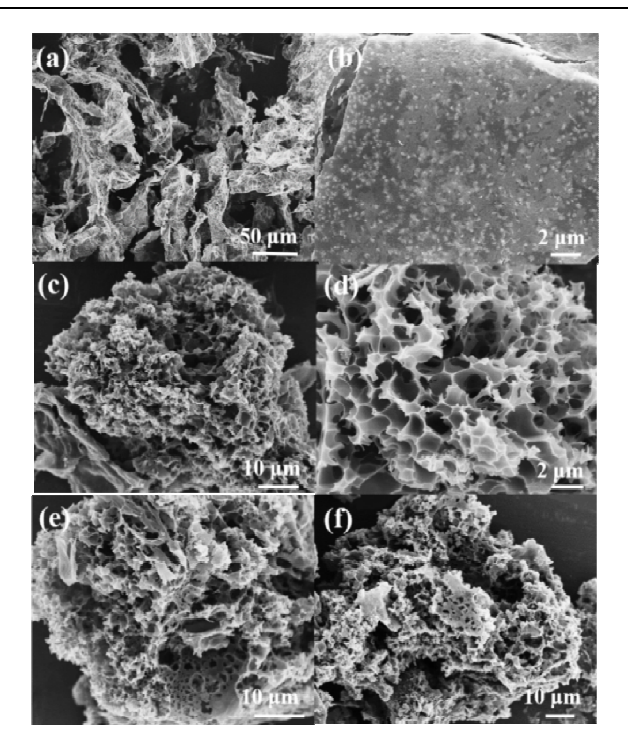


Figure 1. Representative SEM images of the carbon aerogels activated at different temperatures: as-carbonized sample (a, b); and activated samples (c, d) K700; (e) K800 and (f) K900.

The detailed morpholgical and structural properties of porous structure of carbon aerogels were further observed using TEM. Figure 2 exhbits the typical TEM and HRTEM images of carbon aerogels activated at 700 °C. The obtained TEM images are fully consistent with FESEM observations (Figure 2(a)), which demonstrates that the channel wall of porous carbon aerogels are composed by small carbon particles of about 20-40 nm in diameter, which connect together to form mesoporous structure (Figure 1 (c) and (d)). The high resolution TEM image of the selected area shown by square bracket in figure 2 (a) exhibits that there are large number of micropores in the carbon particles (Figure 2 (b)). The diameter of the pores are uniform, and the pore sizes are in the range of 2 ± 1 nm (Figure 2 (b)). The highresolution image of the carbon aerogels also reveals that the aerogels had a highly disordered slothole-like porous carbon structure with a large fraction of micro- and mesopores (Figure 2(c), which facilitates ion transport during charging/discharging process. Figure 2 (c) also exhibited that there are some ordered lattice fringes in the particles, which is from the graphitization of the carbon aerogels to some extent. These TEM images substantially indicate that the activation process etched the carbon aerogels and has significantly tuned porous structure. Thus, from all the morphological characterizations, one can figure out the microstructures of KOH activated carbon aerogels. The KOH activated carbon aerogels have a typical hierarchical porous structure. The first level is very large macropores, which is larger than 50 nm in diameter, the second level is the mesopores in the channel wall of the large pores, which is composited by connection of carbon nanoparticles, and is about 2-50 nm in diameter, and the third level is

micropores in carbon nanoparticles, which is composited by graphite-like structures, and is smaller than 2 nm.

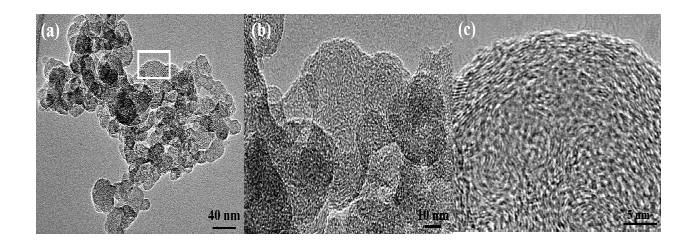


Figure 2. TEM (a) and (b) and HRTEM (c) images of K700 sample.

To evaluate the electrochemical performance of the porous carbon aerogels, cyclic voltammetric (CV) tests were carried out in a three-electrode configuration in an aqueous solution of 6 M KOH, and the results are depicted in Figure 3. Figures 3 (a-d) present CV curves of the four samples at various scanning rates in the potential ranges from -1 to 0 V. As shown in the figures, the CV curves of three-electrode system exhibit an approximately rectangular shape even at the scan rate of 200 mV s⁻¹, indicating a near-ideal capacitive behavior with good rate capability. The slight deviation from the ideal rectangular shape is may due to the ESR (Equivalent Series Resistance) and the pore size distribution of samples. Figure 3 (e) is the CV curves of the four electrodes at the potential scan rates of 2 mV s⁻¹. From Figure 3 (e), one can see that the current density of K700 is the highest compared with other samples, and all samples diaplayed more rectangular shape at the low scan rate. Figure 3 (f) summarizes the gravimetric specific capacitance of the samples according to the CV testing. The prepared carbon aerogels electrode exhibited the lowest specific capacitance and only 88 F g⁻¹ was obtained even at the lowest scan rate of 2 mV s⁻¹. The samples of K800 and K900 displayed increased specific capacitance of 118.8 and 133.6 F g⁻¹

at 2 mV s⁻¹, respectively. Impressively, the specific capacitance of the K700 electrode reached to 268.4 F g⁻¹ at scan rate of 2 mV s⁻¹. These values are much higher than that of the graphene-based macro-mesoporous carbon (226 F g-1 at 1 mV s-1), and twodimensional graphene-based mesoporous carbon sheets (148 F g 1).39,40 Even though capacitance loss can be observed when increasing the scan rate from 2 mV s⁻¹ to 200 mV s⁻¹ for all the carbon samples, the K700 electrode still demonstrates a specific capacitance of as high as 202.1 F g⁻¹.

The Nyquist plot of impedance behavior as a function of frequency is often used to evaluate the frequency response of supercapacitors. Figure S3 shows the impedance curves obtained for different aerogel samples at different frequency ranging from 0.01 Hz to 100 kHz, and a magnified view of the high-frequency region is shown in the inset. Interestingly, it was observed that K700 sample displayed a nearly ideal capacitive behavior with a vertical slope at low frequencies. The ESR (Equivalent Series Resistance) of the samples, i.e., K700, K800, K900, and without activation were, 0.67 Ω , 0.74 Ω , 0.75 Ω , 0.93 Ω , respectively. Generally, ESR contains three different conponents, the contact resistance, solution resistance and the bulk resistance of the electrode. K700 sample has the lowest ESR value, meaning the contact resistance and the bulk resistance is very low. This may be the reason that the current density of K700 sample shown in CV profiles is higher than those of K800 and K900. ESR data determines the rate that the supercapacitor can be charged and discharged, and it is a very important factor to determine the power density of a supercapacitor. 41 Hence, it is believed that the electrochemical performance of as-prepared carbon aerogels can be improved dramatically by activation process.

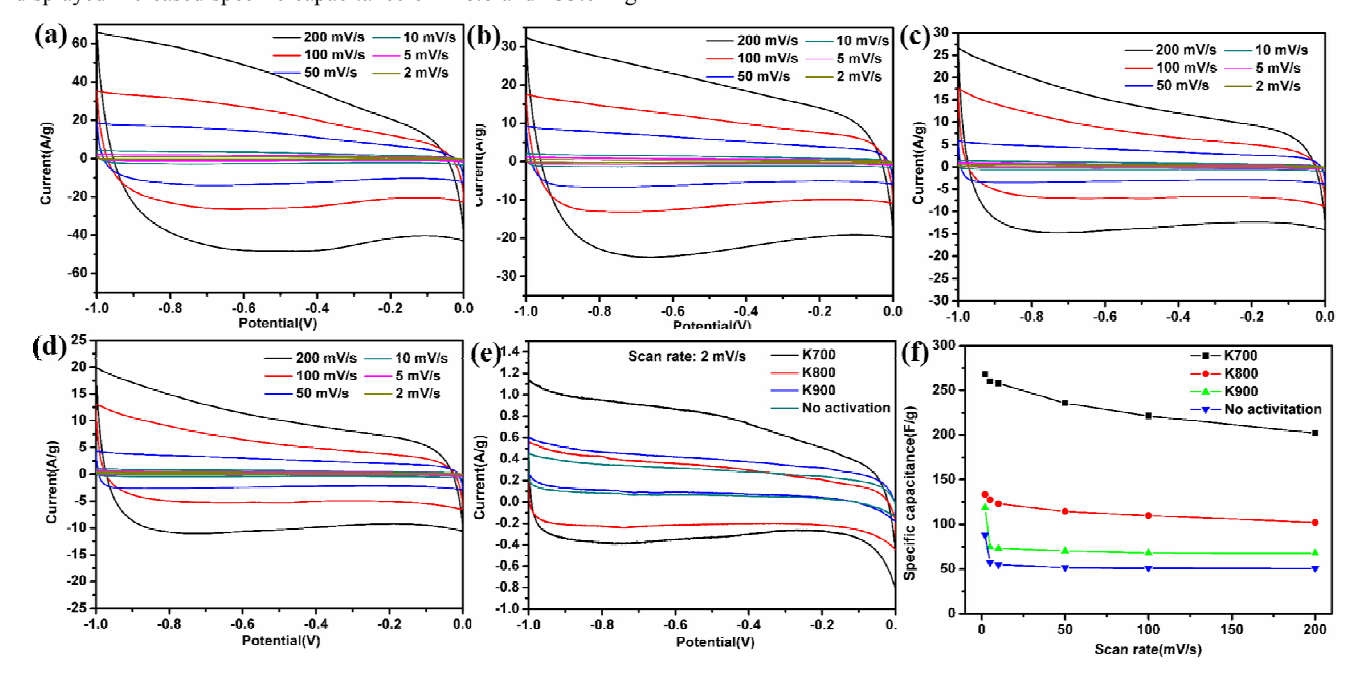


Figure 3. (a-d) CV curves of the porous carbon aerogels electrodes at varied potential scan rates in 6 M KOH aqueous solution ((a) K700; (b) K800; (c) K900; (d) No activation); (e) CV curves of the four electrodes at the potential scan rates of 2 mV s⁻¹; (f) Specific capacitances of the four electrodes as a function of scan rate derived from (a-d).

Cite this: DOI: 10.1039/c0xx00000x

www.rsc.org/xxxxxx

ARTICLE TYPE

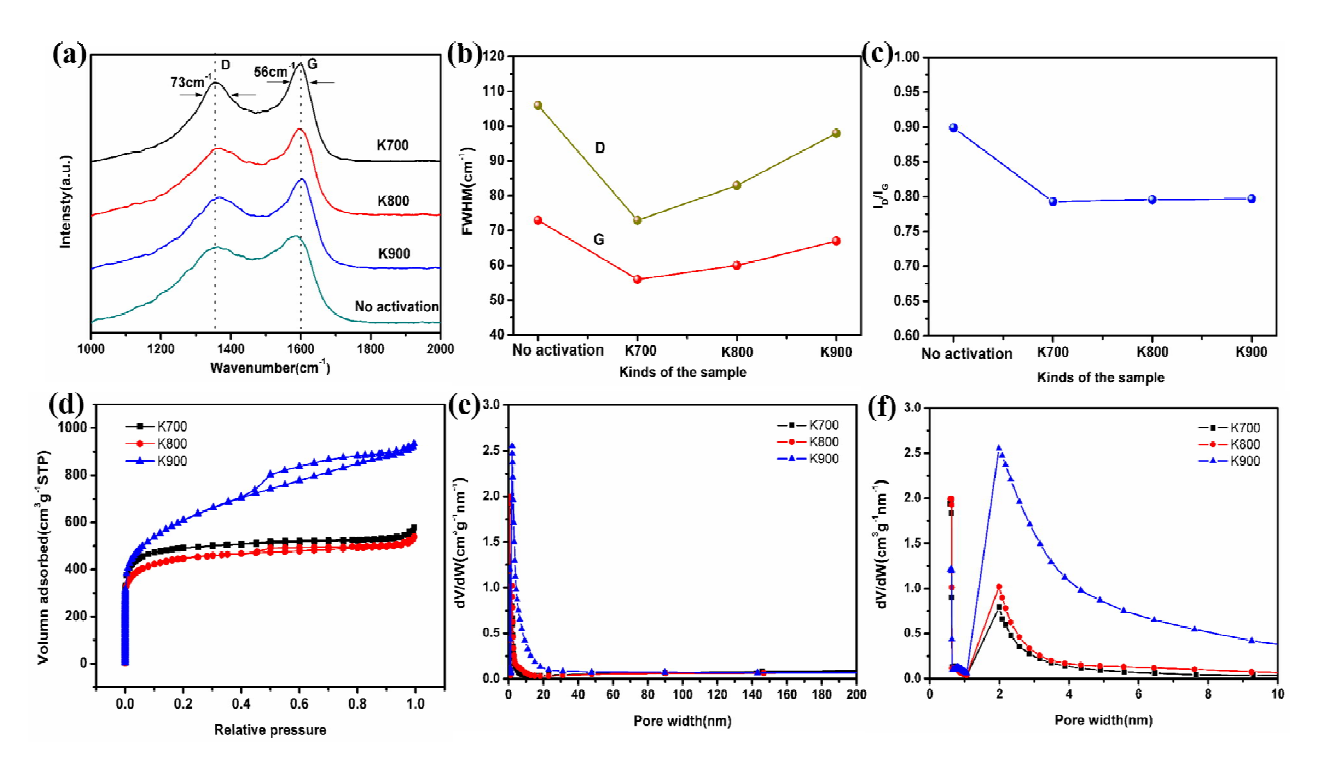


Figure 4. (a) Raman spectra of the pristine and activated samples; (b) full width at half maximum (FWHM) of the D- and G-band peaks; (c) ratio of integrated intensities of the D- and G-bands (I_G/I_D); (d) Nitrogen adsorption/desorption isotherms of the samples; (e) Pore size distribution for N₂ (calculated by using the BJH model); (f) Detail view of (e).

The enhancement of the specific capacitance of the activated samples is suggested to be related to the degree of graphitization and the increase of the surface area and the manipulation of pore size and distribution, further demonstrated by Raman-scattering measurements and N₂ adsorption/desorption experiments.

Raman-scattering measurements were carried out to understand the structural evolution of the modified carbon aerogels activated at different temperatures. Figure 4 (a) shows the Raman spectra of all the samples prepared at various activation temperatures. For comparison, the Raman-scattering result for carbon without activation is also displayed in the spectra. All the samples exhibited two distinct peaks located at 1350 cm⁻¹ and 1582 cm⁻¹ which are indexed to the D band and G band vibrations, respectively. The D band reflects the disordered carbon, while the G band is caused by the vibration of ordered carbon. 42,43 It was found that both the D and G bands of carbon without activation display broad shape and low intensity, indicating the possible high concent of amorphous carbon. Figure 4 (b) shows the full width at the half maximum (FWHM) values of the D-band and G-band of the samples, which reveals that the FWHM values of the D- and G-bands of carbon after activation are lower than that without activation, indicating a sharper feature of peaks. The Dand G bands of activated carbon aerogels show sharper and high intensity peaks which indicate the improved graphite degree after activation in the samples. This conclusion is further demonstrated by the intensity ratio (I_D/I_G) of D- and G bands, which reflects the ratio of disordered carbon and ordered carbon in the carbon aerogels (Figure 4 (c)). The values of I_D/I_G for activated carbon aerogels decreases to less than 0.8, indicating very high content of ordered carbon in the activated carbon aerogel samples. The increased content of ordered carbon indicated that the post activation process not only can expect to create pores, but also can really enhance the graphite degree. The slight increase of I_D/I_G after activation temperature at 800 and 900 °C indicated that the degree of graphitization in the sample activated at 700 °C is the highest while graphitization decreases with increasing the activation temperature. The improved graphite degree of activated carbon aerogels can siginificantly increase the electric conductivity, which should decrease the equivalent seriers resistance of supercapacitors, consistenting with the results of impedance behaviour. The FTIR spectra of carbon aerogels activated at different temperatures are also shown in Figure S4. There is no obvious peak located at the spectra, indicating that the prepared carbon aerogels are very clean and there is no any other element or residual organic compound existed in the samples except C. The mechanical property of the carbon aerogels is also perfect. Figure S5 (a) shows a photograph of a carbon aerogel supporting a mass of 50 g with no deformation. In addition, as shown in Figure S5 (b), we put a carbon aerogel on the spider web to illustrate the light weight originated from high porosity of the sample.

Figure 4 (d) exhibits the typical N_2 adsorption/desorption isotherms of all samples. As illustrated in Figure 4 (d), the type-IV nitrogen sorption isotherms for the samples suggest the existence of different pore sizes from micro- to macropores. Major adsorption of the samples occurs at low relative pressure of less than 0.1, giving rise to an almost horizontal plateau at higher relative pressures. These curves indicated that the samples possess high microporosity. Furthermore, the hysteresis between adsorption and desorption branches (at 0.5-1.0 P/P $_0$) of the samples also suggest the existence of different types of pores with no pore-blocking effect during desorption. This result can be demonstrated by the pore size distribution calculated from the BJH model, shown in figure 4 (e) and (f). Figure 4 (e) and (f) demonstrate that all the three samples have both mesopores (2-50

nm) and micropores (< 2 nm). The mesopores have a pore size of \sim 2 nm for the three samples which is fully consistent with the observed HRTEM image, and the sizes of the micropores are typically centered at 0.6 nm. Table 1 summarizes the specific surface area and pore volumes of samples. After the activation with KOH etching, the specific surface area is amplified to 2064.79 m² g⁻¹. The specific surface area and total pore volume of K700 is lower than that of K900 while the micropore volume of K700 sample is typically the highest with proper mesopore volume. The micropore volume of K900 sample is the lowest value with the highest surface area and mesopore volume, indicating that the increase of the specific surface area can not always positively enhance the specific capacitance.

Table 1. Physical properties and specific capacitance obtained from CV scaning at 2 mV/s in the three electrode testing. Cs is defined as the capacitance obtained at scan rate of 2 mV/s. The rate capability (R) is defined as the ratio of the capacitance value obtained at 100 mV/s to that at 2 mV/s.

Sample ID	Specific surface area	Total pore volume	Micropore volume	Mesopore volume	Specific capatance C _s	Rate capability
	$cm^2 g^{-1}$	$cm^3 g^{-1}$	$cm^3 g^{-1}$	$cm^3 g^{-1}$	F g ⁻¹	R
Variable	X_1	X_2	X_3	X_4	X_5	X_6
K700	1892.4	0.86	0.58	0.23	268.4	82.5%
K800	1641.6	0.80	0.46	0.27	133.6	82.3%
K900	2064.8	1.41	0.28	1.0	118.8	57.4%

To further investigate the relationship between porous structure and elecrochemical performance of electrode materials, correlation analysis is conducted based on the results of N_2 adsorption/desorption and cyclic voltammetric (CV) tests. The Correlation, indicating the related degree of variable, can be calculated using the following equation:

$$\textit{Correlation}(x,y) = \frac{n\sum (xy) - \sum x\sum y}{\sqrt{\left[(n\sum x^2 - (\sum x)^2) \bullet (n\sum y^2 - (\sum y)^2)\right]}} \ensuremath{\text{(1)}}$$

Where x and y are variable, and n is the number of x or y. The calculated Correlation(X₅, X₃) and Correlation(X₅, X₄) equal to 85% and 61%, suggesting that the specific capacitance is highly relayant with micropore volume and only moderately associated with mesopore volume. The increase of micropore volume can enhance the specific capacitance of electrode materials effectively, while increasing mesopore volume can do little. The Correlation(X₆, X₃) and Correlation(X₆, X₄) are calculated to be 92% and 99%, repectively, indicating that rate capability is mainly associated with the mesoporous volume of materials. The correlation analysis results show that the micropores and mesopores play different roles on electrochemical properties of the electrode materials and the energy storage capacity is determined by micropore volume, while the rate capability is mainly decided by mesopore volume. When electrolyte ions immerse into the pores, the distance between the electrolyte ions and micropore walls on both sides are the shortest, indicating the strongest electrostatic adsorption which lead to the best energy storage capacity. However, mesopores mainly store electrolyte to shorten the electrolyte ions diffusion distance, at the same time, can supply electrolyte ions in the process of charging and discharging quickly. For ideal ECs electrode materials, it should have a hierarchical porous structure. K700 sample typically has three types of pores, i.e., micropore (< 2 nm), mesopores (2-50 nm) and macropores (> 50 nm), indicating a hierarchical porous

structure, which is consistent with the observed FESEM and TEM results.

Above all, electrochemical properties of a porous carbon electrode material is not always directly proportional to its specific surface area. Aside from specific surface area, effective pore size distribution, good electrical conductivity (to improve the power density) are also effects the performance of supercapacitors. Combined all those factors, one can understand that why K700 sample shows the best electrochemical performance.

The special hierarchical porous structure is attributed to the reaction between KOH and carbon in the aerogels during the activation process. 44,45 As mentioned in experimental section, the activation process occurred at high temperature treatment of assynthesized carbon aerogels and KOH penetrated in the pores of the carbon aerogels. At high temperature, the reaction between carbon on the surface of the wall of the channel of aerogels and KOH can occur as Formula (2)

$$4 KOH + C \rightarrow K_2 CO_3 + K_2 O + 2 H_2$$
 (2)

This reaction preferentially happens on the surface of the wall of channel in as-synthesized carbon aerogels, and the surface can be corroded to form nanopores. From the Raman-scattering results, it is clear that the as-carbonized aerogels possess certain extent of graphitization. Normally, the low graphitized part can be corroded first, and leave higher graphitized nanoparticles. This is why the hierarchical porous structure can be formed after activation process, and why the graphite peak of the activated sample is much higher than unactivated carbon aerogels. By increasing the activation temperature, the reaction between carbon and KOH becomes more violent and KOH can react with the more graphitized area in carbon particle which cause the decrease of peaks of graphite in Raman spectra. It is known that the conductivity of carbon aerogel is related to the degree of graphitization of the sample. Therefore, the conductivity of the

sample K700 should be the highest one, because of the highest graphitization degree in the sample activated by KOH at 700 °C which is fully consistent with the ESR results.

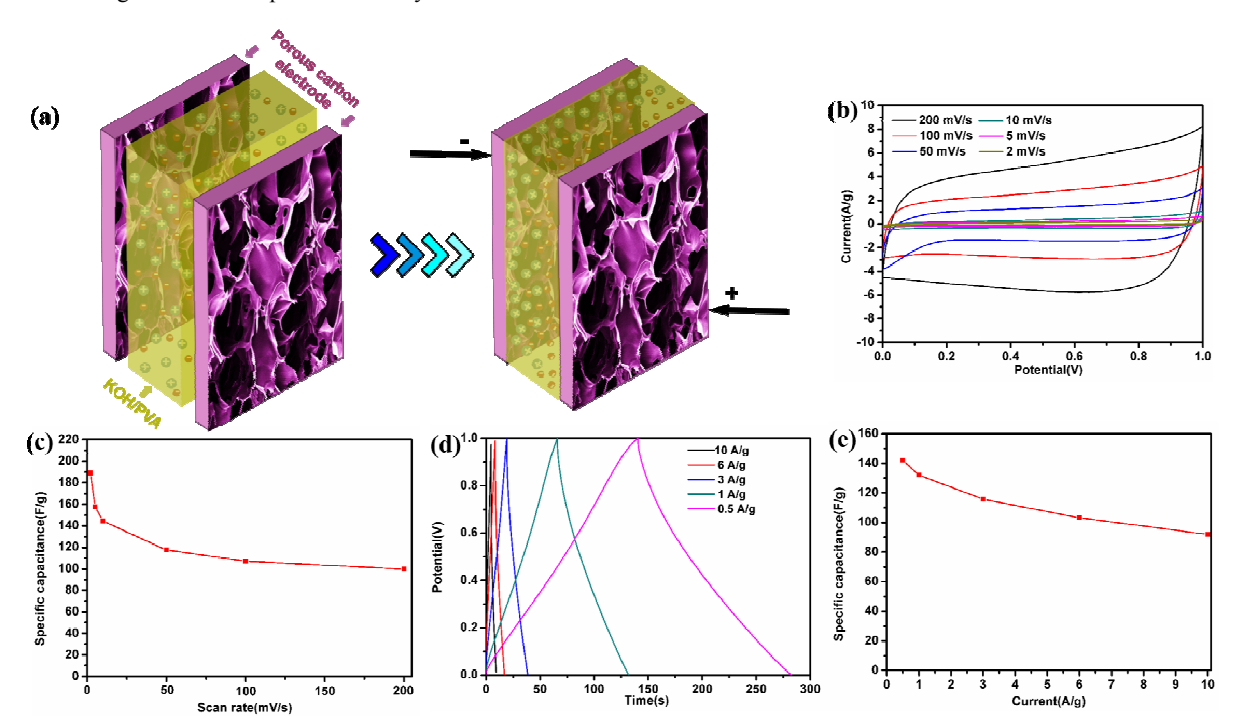


Figure 5. (a) Schematic of the fabricated hierarchical porous carbon supercapacitor; (b) CV curves of K 700 sample; (c) specific capacitance of K700 sample as a function of scan rate derived from (b), (d) charge-discharge curves of K700 sample at different current densities, and (e) specific capacitance of K700 sample as a function of current density derived from (d).

As we known, electrolyte plays an important role in supercapacitor, the potential range and ionic conductivity of the electrolyte can influence supercapacitor behavior obviously. Many reports are based on liquid electrolytes because of the high ionic conductivity of them. However, there are also many existed disadvantageous in the liquid electrolytes, such as low potential range, leakage, corrosion and explosions. Therefore, replacing liquid electrolytes with solid electrolytes in supercapacitor has been explored by many researchers. The solid electrolytes have several advantages over liquid ones that includes easy handling without leakage and thus making it environmentally safe, low internal corrosion, flexibility in packaging etc. 46 In order to assess the reliable electrochemical performance of the carbon aerogels, a two-electrode solid state symmetrical supercapacitor device was assembled to characterize the electrochemical storage capability of K700 sample in KOH/PVA solid electrolyte. Figure 5 (a) shows the schematic of all-solid-state symmetric supercapacitor using hierarchical porous carbon supercapacitor. The porous carbon based cell was constructed by sandwiching a KOH/PVA gel electrolyte with two pieces of as prepared carbon electrodes via a facile and effective process as discussed in experimental section. The CV curves at various potential scan rates ranging from 2 to 200 mV s⁻¹ and galvanostatic charging/discharging curves as a function of current density derived from 0.5 to 10 A g were investigated, respectively. As shown in Figure 5 (b), the CV curves at various scan rates are rectangular-like in shape and symmetric from 0 to 1 V, indicating a near-ideal capacitive behavior with good rate performance. The highest specific capacitance reaches to 189 F·g⁻¹ at 2 mV s⁻¹ and decreases to 99.8

F g⁻¹ at 200 mV s⁻¹ (Figure 5 (c)). The galvanostatic chargedischarge curves (Figure 5 (d)) at various current densities showed good symmetry, nearly linear slopes and quick currentvoltage response, which confirms the good supercapacitor characteristics for K700 sample. The calculated specific capacitances from the discharge curves are shown in figure 5 (e). The specific capacitance at 0.5 A g⁻¹ is about 142.1 F g⁻¹, which is much higher than the electrode prepared from banana using KOH activation (65 F g⁻¹).⁴⁷ A IR drop of 0.02 V can be obtained at 0.5 A g⁻¹, indicating a negligible leakage current of the sample. In addition, The CV curves of two-electrode supercapacitor using liquid electrolyte at various potential scan rates ranging from 2 to 200 mV s⁻¹ were also also investigated. As shown in Figure S6, the CV curves at various scan rates are rectangular-like in shape, indicating a near-ideal capacitive behavior with good rate capability.

The electrochemical impedance spectra was also conducted from 0.01 Hz to 100 kHz for the solid and liquid electrolyte supercapacitors, as shown in Figure S7. It was found that the ESR of K700 using solid electrolyte is about 0.76 Ω , which is similar to that of aqueous electrolyte about 0.72Ω . While the charge transfer resistance showed significant difference and this value for solid electrolyte was about 5.4 Ω , much higher than that for aqueous electrolye about 2.6 Ω . At low frequency range, a nearly vertical line can be observed, indicating the ideal supercapacitve feature of the symmetrical supercapacitor. The results of EIS of the symmetrical supercapacitor indicated that K700 sample had the best supercapcitive performance.

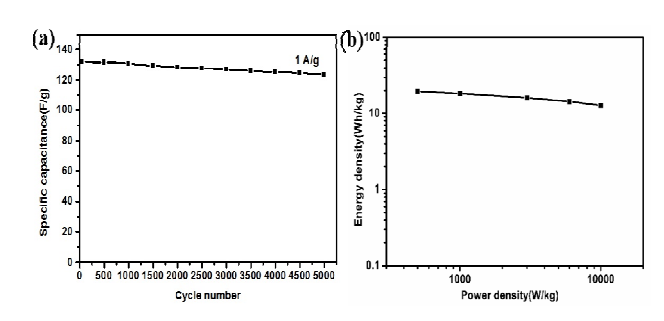


Figure 6. (a) Cycle performance and Coulombic efficiency at 1 A g⁻¹ over 5000 cycles and (b) Ragone plots of K700 sample.

To assess the cycling stability of K700 for supercapacitor application, the galvanostatic charge-discharge experiement was performed for 5000 cycles. Figure 6 (a) shows the cycling stability of the symmetric electrodes at a constant charge and discharge current density of 1 A g⁻¹ for 5000 cycles. The Coulombic efficiency retained about 93.86% with a small decrease from 132 to 123.9 F g-1, indicating an excellent cyclability of the symmetric cell based on the hierarchical porous carbon aerogels. The power density and energy density of the symmetric supercapacitor is shown in a Ragone plot (Figure 6 (b)). Benefitting from a high specific capacitance of up to 142.1 F g⁻¹ (obtained at a current density of 0.5 A g⁻¹) and an operating voltage of 1 V, the cell displayed the energy density of ~19.74 Wh kg⁻¹ and a power density of 0.5~ kW kg⁻¹. Although compared with a few individual cases prepared from the carbonization of mixtures of organic reagents, electrochemical performance of K700 sample is not an outstanding one, but the requirement of highly toxic organic reagents can discourage their use in electrode preparation. Thus, the presented work is highly promising if one can consider the availability of bagasse as a biomass waste and the ease of the preparation method.

4. Conclusions

In summary, a supercapacitor electrode material with excellent performance has been achieved by carbonization of cellulose aerogels using bagasse, an industrial waste, and activation with KOH. The resulting carbon aerogels have macro, meso, and micro hierarchical porous structures and possess extremely high specific surface area of 1892.4 m² g⁻¹. The specific capacitance calculated from the charge-discharge experiments using a symmetric supercapacitor was about 142.1 F g⁻¹ at 0.5 A g⁻¹ with excellent capacitance retention at ~93.86% over 5000 cycles, which translates into the highest energy density of ~19.74 Wh kg ¹ and a power density of 0.5~ kW kg⁻¹. The obtained results demonstrate the possibility for the large scale production of hierarchical porous carbons by choosing low-cost biomass waste, i.e. bagasse as the raw material. The presented synthesis method also opens a new approach for the large-scale production of carbon electrodes that are especially suitable for supercapacitors.

Acknowledgements

The authors are thankful for fundings from the National Natural Science Foundation of China (Grant No. 51372142), Innovation Research Group (IRG: 51321091) and the "100 Talents Program" of the Chinese Academy of Sciences. Thanks for the support from the "thousands talents" program for pioneer researcher and his innovation team, China.

Notes

- ^a State Key Laboratory of Crystal materials, Shandong University, Jinan 250100, P. R. China. E-mail: hongliu@sdu.edu.cn.
- b Institute of Chemical Materials, China Academy of Physical engineering, Mianyang, 621900, PR China
- ^c School of Materials Science and Engineering, Georgia Tech, Atlanta, GA 30032. E-mail: cp.wong@mse.gatech.edu.
- ^dDepartment of Chemistry, Faculty of Science and Arts, Najran University, Najran-11001, Kingdom of Saudi Arabia
- ^e Promising Centre for Sensors and Electronic Devices (PCSED), Najran University, Najran-11001, Kingdom of Saudi Arabia

E-mail: ahmadumar786@gmail.com

Electronic Supplementary Information (ESI) available, See DOI: 10.1039/b000000x/

* Corresponding authors.

‡ Pin Hao and Zhenhuan Zhao contributed equally to this work.

References

- Z. Wu, K. Parvez, X. Feng and K. Müllen, Nat. Commun., 2013, 4,
- P. Simon and Y. Gogotsi, Nat. Mater. 2008, 7, 845-854.
- P. Sharma and T.S. Bhatti, Energy Convers. Manage., 2010, 51,
- A. Stein, Z. Wang and M.A. Fierke, Adv. Mater., 2009, 21, 265-293.
- Y. Gogotsi and P. Simon, Sci. Magazine, 2011, 334, 917-918.
- L. Mao, K. Zhang, H.S.O. Chan and J. Wu, J. Mater. Chem., 2012, **22**. 1845-1851.
- J. Sun, W. Li, B. Zhang, G. Li, L. Jiang, Z. Chen, R. Zou and J. Hu, Nano Energy, 2014, 4, 56-64.
- R. Ramya, R. Sivasubramanian and M.V. Sangaranarayanan, Electrochim. Acta, 2013, 101, 109-129.
- K. Wang, H. Wu, Y. Meng and Z. Wei, Small, 2014, 10, 14-31.
- P. Sharma and T.S. Bhatti, Energy Convers. Manage., 2010, 51, 2901-2912.
- Z. Niu, H. Dong, B. Zhu, J. Li, H. H. Hng, W. Zhou, X. Chen and S. Xie, Adv. Mater., 2013, 25, 1058-1064.
- J. Li, X. Wang, Y. Wang, Q. Huang, C. Dai, S. Gamboa and P.J. Sebastian, J. Non-Cryst. Solids, 2008, 354, 19-24.
- Z. Niu, L. Zhang, L. Liu, B. Zhu, H. Dong and X. Chen, Adv. Mater., 2013, **25**, 4035-4042.
- Q. Cheng, J. Tang, J. Ma, H. Zhang, N. Shinya and L.C. Qin, J. Phys. Chem. C, 2011, 115, 23584-23590.
- J. Yan, T. Wei, Z. Fan, W. Qian, M. Zhang, X. Shen and F. Wei, J. Power Sources, 2010, 195, 3041-3045.
- Z. Niu, P. Luan, Q. Shao, H. Dong, J. Li, J. Chen, D. Zhao, L. Cai, W. Zhou, X. Chen and S. Xie, Energy Environ. Sci., 2012, 5, 8726-8733
- C. Liu, Z. Yu, D. Neff, A. Zhamu and B.Z. Jang, Nano Lett., 2010, 10. 4863-4868.
- C.X. Guo and C.M. Li, Energy Environ. Sci., 2011, 4, 4504-4507.
- Z. Niu, J. Chen, H. H. Hng, J. Ma and X. Chen, Adv. Mater., 2012, 24. 4144-4150
- B. Subhadra, Energy Sci. Tech., 2013, 5, 36-49.
- A.A. White, M.S. Platz, D.M. Aruguete, S.L. Jones, L.D. Madsen and R.D. Wesson, ACS Sus. Chem. Eng., 2013, 1, 871-877.
- H. Wang, E. Zhu, J. Yang, P. Zhou, D. Sun and W. Tang, J. Phys. Chem. C, 2012, 116, 13013-13019.
- L. Wei, M. Sevilla, A.B. Fuertes, R. Mokaya and G. Yushin, Adv. Energy Mater,. 2011, 1, 356-361.
- H. Sun, L. Cao and L. Lu, Energy Environ. Sci., 2012, 5, 6206-6213.

- 25 W. Sia, J. Zhou, S. Zhang, S. Li, W. Xing and S. Zhuo, Electrochim. Acta, 2013, 107, 397-405.
- 26 Y. Liang, D. Wu and R. Fu, Scientific reports, 2013, 3, 1119.
- O. Inganäs and S. Admassie, Adv. Mater., 2013, 26, 830-848.
- 28 Q. Wang, Q. Cao, X. Wang, B. Jing, H. Kuang and L. Zhou, J. Power Sources, 2013, 225, 101-107.
- 29 Y. Lv, L. Gan, M. Liu, W. Xiong, Z. Xu, D. Zhu and D.S. Wright, J. Power Sources, 2012, 209, 152-157.
- E. Raymundo-Piñero, F. Leroux and F. Béguin, Adv. Mater., 2006, 18, 1877-1882.
- Z. Gui, H. Zhu, E. Gillette, X. Han, G.W. Rubloff, L. Hu and S.B. 31 Lee, ACS Nano, 2013, 7, 6037-6046.
- Y. R. Kang, Y. L. Li, F. Hou, Y. Y. Wen and D. Su, Nanoscale, 2012, 32 4, 3248-3253.
- H. Zhu, Z. Jia, Y. Chen, N. Weadock, J. Wan, O. Vaaland, X. Han, T. 33 Li and L. Hu, Nano Lett., 2013, 13, 3093-3100.
- Y. Zhu, S. Murali, M. D. Stoller, K. J. Ganesh, W. Cai, P. J. Ferreira, A. Pirkle, R. M. Wallace, K. A. Cychosz, M. Thommes, D. Su, E. A. Stach and R. S. Ruoff, Sci., 2011, 332, 1537-1541.
- M. Zhi, C. Xiang, J. Li, M. Li and N. Wu, Nanoscale, 2013, 5, 72-
- D. Bhattacharya, L.T. Germinario and W.T. Winter, Carbohydr. Polym., 2008, 73, 371-377.
- M. Yang, Y. Zhong, L. Su, J. Wei and Z. Zhou, Chem. Eur. J., 2014, 37 20, 1-9,
- L. Szcześniak, A. Rachocki and J. Tritt-Goc, Cellul., 2008, 15, 445-38 451.
- 39 Z. S. Wu, Y. Sun, Y. Z. Tan, S. Yang, X. Feng and K. Mullen, J. Am. Oil Chem. Soc., 2012, 134, 19532-19535.
- S. Yang, X. Feng, L. Wang, K. Tang, J. Maier and K. Müllen, Angew. 40 Chem. Int. Ed., 2010, 49, 4795-4799.
- 41 Q. Cheng, J. Tang, J. Ma, H. Zhang, N. Shinya and LC Qin, Carbon, 2011, 49, 2917-2925.
- A. Jänes, H. Kurig and E. Lust, Carbon, 2007, 45, 1226-1233. 42
- 43 F. Bonhomme, J. C. Lassèguesz and L. Servant, J. Electrochem. Soc., 2001, 148, 450-458.
- G. G. Stavropoulos, Fuel Process. Technol., 2005, 86, 1165-1173.
- H. Wang, Z. Li, Y. Huang, Q. Li and X. Wang, J. Mater. Chem., 2010, 20, 3883-3889
- 46 G. Ma, J. Li, K. Sun, H. Peng, J. Mu and Z. Lei, J. Power Sources, 2014, 256, 281-287.
- 47 V. Subramanian, C. Luo, A. M. Stephan, K. S. Nahm, Sabu Thomas and B. Wei, J. Phys. Chem. C, 2007, 111, 7527-7531.